Received: 13 March 2022 | Revised: 3 July 2022 | Accepted: 17 July 2022

DOI: 10.1111/jace.18697

Journal of the American Ceramic Society

RESEARCH ARTICLE

Recycled ZnO-fused macroporous 3D graphene oxide aerogel composites for high-performance asymmetric supercapacitors

Kamrul Hassan[1,2] | **Rumana Hossain**[1] | **Veena Sahajwalla**[1]

[1]Centre for Sustainable Materials Research and Technology, SMaRT@UNSW, School of Materials Science and Engineering, UNSW Sydney, Sydney, Australia

[2]School of Chemical Engineering and Advanced Materials, The University of Adelaide, Adelaide, South Australia, Australia

Correspondence
Rumana Hossain, Centre for Sustainable Materials Research and Technology, SMaRT@UNSW, School of Materials Science and Engineering, UNSW Sydney, Australia.
Email: r.hossain@unsw.edu.au

Funding information
Australian Research Council's Industrial Transformation Research Hub, Grant/Award Number: IH190100009

Abstract

In the arena of energy storage device, asymmetric supercapacitors (ASCs) are considered a key category due to its high-power density and energy densities. In this study, a novel macroporous microrecycled ZnO nanoparticles (mi-ZnO NPs) recovered from spent Zn–C battery-decorated three-dimensional graphene aerogel (GA) composite has been synthesized via simple eco-friendly synthetic method, which is used as a proficient anode material to fabricate ASC. The interconnected macroporous networks and ~40-nm microrecycled ZnO NPs incorporated GA (mi-ZnO–GA) enhanced the surface area of anode materials, which lead to achieve a formation of high-performance ASC. Here, we composed ASCs from a microrecycled ZnO thin film (cathode) and mi-ZnO–GA composite (anode), which reveals fast charging/discharging characteristics, stable widen cell voltage, superior power, and energy densities (13.7 W h/kg, 13.2 kW/kg), and finally stable cyclability (76.8% retention after 5000 cycles). These outcomes open up the window for microrecycled ZnO NPs incorporated GA (mi-ZnO–GA) as a prominent anode material for high-performance energy storage devices.

KEYWORDS

anode materials, asymmetric supercapacitors, microporous mi-ZnO/graphene aerogel, microrecycled ZnO nanoparticles

1 | INTRODUCTION

Supercapacitors (SCs) are a developing technology that links the properties of capacitors and conventional batteries, filling a critical gap in today's rapidly changing needs for energy storage. SCs can be used in a broad range of applications such as electric vehicles, pacemakers, and portable electronics[1,2] with attractive properties like high-power density, cycle stability, and quick charge–discharge rate.[3–5] For its prevalent use, the improvement of the energy density of SCs is an important factor. The equation $E = 1/2CV^2$ can be used to determine energy density of an SC, where E is the energy density, C is the capacitance of the cell, and V is the the cell voltage.[6,7] The exponent of the equation signifies an improvement of the energy density of the capacitor. First, using the ionic or organic electrolytes elevates the voltage to 3 V.[8,9] However, this method is unfavorable because of its high cost, low ionic conductivity, the

toxicity of organic electrolytes, and the limitations of the working temperature of ionic liquid electrolytes. Second, the production of electrolyte-based (aqueous) asymmetric SCs (ASCs) comprising a Faradic battery–type cathode as a source of energy and a capacitor-type anode as a source of power.[10,11] An ASC holds the advantage of the various voltage windows of the anode and the cathode equally such that it is possible to effectively obtain an enhanced operating voltage in a cell device, resulting in an enhanced basic capacitance and dramatically increased energy density.

Several efforts have been made to develop cathodic materials, for examples, MnO_2,[12] NiO,[13] $Ni(OH)_2$,[14] and CoO_x[15]. Besides, carbon-based materials, including activated carbon,[16] carbon nanofiber,[17] carbon nanotube,[18] and grapheme,[19] usually used as an anode material in ASCs. Graphene has distinguished itself among them because of its outstanding features such as wide surface area, processability of the solution, good electrical conductivity, excellence in the mechanical behaviors, and improved electrochemical steadiness.[20,21] However, due to the agglomeration of graphene nanosheets,[21,22] substantial surface area losses are usually observed while processing, resulting in a decreased electrochemically active surface that significantly limits the basic capacitance. The manufacture of graphene nanosheets into such a graphene aerogel (GA) seems to be a useful concept; a robust three-dimensional (3D) network that can potentially impede graphene nanosheet aggregation.[23] The accessible 3D network architecture of the GA electrodes gives additional large surface area, whereas the crystalline structure (10-mm pore size) facilitates the efficient transport of electrolyte ions.[24] One relevant drawback is that the method of oxidation–reduction reduces electrical properties compared to pristine graphene leading to the advancements of defect sites.[25] Therefore, producing a GA with improved electrical conductivity is beneficial. GA activation with metallic nanoparticles enhances the mass electrical conductivity by preferentially anchoring metallic nanoparticles at rather electrical inhibiting defects sites[26,27] and decreases the composite's working function.[28]

In this research, for energy storage devices, ZnO nanoparticles produced from spent Zn–C batteries were used to produce composite hybridized compounds. Electronic waste (e-waste) seems to have become the fastest growing disposal stream[29] because of the shortened lifetime of electronic devices and frequent improvements to more sophisticated ones. Energy storage systems such as batteries are commonly used and make a big contribution to the overall e-waste amount. Requirement for batteries is expected to rise annually by 7.7%, with a size of the market in 2019 hitting US$120 billion.[30] Per year, about 350 million batteries are being used in Australia. Many of the batteries used (about 98%) by disposable handheld devices are Zn–C battery, and around 19% of which are Zn–C battery packs. Zn–C batteries are non-rechargeable and are therefore disposed of or landfilled by a large number of Zn–C batteries.[30] In devices like remote controls, radios, and alarm clocks, Zn–C batteries are commonly used. Significant amounts of manganese and zinc are part of the Zn–C battery structure. It is very important to recycle those precious metals from recycled batteries to retain valuable resources, and to protect the environment and to prevent threats to human health. By eliminating the energy-intensive extraction and refining of ore materials, collecting metals from hazardous waste can also reduce the demand of virgin materials and save energy. Several researchers have investigated the recovery of precious metals, particularly Zn and Mn, from e-waste utilizing alkaline and acidic digestion in hydrometallurgical approaches in recent studies.[31,32] Few researchers have also investigated the restoration of ZnO by chemical and hydrothermal approaches.[33] Nevertheless, further dissolvable material recovery and electrochemical developments are needed to retrieve valuable items through hydrometallurgy procedures. Pyrometallurgical methods require high use of resources but have fewer processing steps that enable the use of less challenging methods to recover e-waste value-added resources. High temperatures (1550°C) are used for the recovery of Zn and Mn alloys[31] by the current pyrometallurgical method. In addition, most research attention was focusing on the investigations for the recovery of ZnO with properties indicating the prospect of repurposing ZnO for future applications such as sensors and energy storage systems.[30,34,35]

In this study, we report a novel technique of fabricating nano-ZnO incorporated aerogel graphene to fabricate an enhanced surface area electrode material for ASCs. In this eco-friendly synthesis technique, recovered nano-ZnO particles from wasted Zn–C batteries are integrated into the GA 3D network (denoted by mi-ZnO–GA) that shows synergetic interplay in between graphene and ZnO at the time of ion transportation. Further, fabricated ASCs composed of a microrecycled ZnO thin film as a cathode and mi-ZnO–GA as an anode demonstrate fast charging/discharging characteristics, stable broaden cell voltage, as well as enhanced columbic efficiency. In addition, we have also calculated power density and energy density for this as-fabricated ASCs, which emphasizes the importance of mi-ZnO–GA materials for the energy storage devices with an outstanding performance.

2 | EXPERIMENTAL DETAILS

Synthesis of ZnO nanoparticles, thin film (ZnO) recycled from Zn–C battery, a synthesis technique of ZnO

nanoparticles–integrated GA 3D microstructure, and the fabrication of ASC have been described in the following subsections.

2.1 | Preparation and characterization of recycled ZnO nanoparticles from waste Zn–C batteries

In order to separate the metallic cover, casing metal (Zn), metal cap, powder materials, carbon rod, and separators postconsumer Zn–C batteries were physically disassembled. The powdered compounds were centrally positioned as conductors as in battery and were squeezed between the two electrodes, whereas the negative electrode was used as a Zn metal casing. Powder substances containing primarily manganese dioxide and zinc chloride as the electrolyte were composed of the positive electrode. The electrolyte-drenched positive terminal powder was used to produce ZnO NPs as fundamental materials. They were held in the oven for 2 h at the temperature of 100°C in order to extract moisture from the powder particles. In the experiment, a horizontal style quartz tube furnace (1000-mm length × 45-mm diameter) with the capability to retain the specimen in a graphite rod and an exterior gas supply device attachment was used. In this procedure, the exterior gas was argon, and 1 L/min was the flow rate of the argon through the heating chamber. Before being inserted into the furnace, moisture-free powder was moved into a ceramic crucible and placed on the graphite-rod sample holder. The ceramic crucible and the graphite rod were then slowly forced for 1 h into the furnace's hot zone (~900°C). The solid grayish material attached to the furnace quart tube in the low-temperature region (280 ± 20°C) near the gas supply outlet was extracted after the heating phase by means of a manual extraction technique. To remove the other hydroxide impurities, the grayish powder obtained from the quartz tube horizontal furnace was kept in a heated condition (500°C). Past investigations have identified an overall process for the growth of ZnO NPs and material characteristics from spent Zn–C batteries.[30,34,35]

2.2 | ZnO thin film on an Ni substrate using a green chemical vapor deposition (G-CVD) technique

The experiment condition for manufacturing a microrecycled ZnO thin film on an Ni substrate by a chemical vapor deposition (CVD) technique was very similar to the synthesis condition of microrecycled ZnO NPs synthesis from spent Zn–C battery. However, slight modification was required, including the ceramic crucible, which was sealed with a ceramic sheet, and the Ni substrate was put in the crucible together with the recovered powdered battery. In our previous study,[35] we documented the brief experimental technique and mechanism for generating ZnO thin film and component characteristics recycled from the cast-off Zn–C batteries.

2.3 | Graphene oxide (GO) synthesis from graphite

Graphene oxide (GO) was manufactured from graphite (Uley, South Australia)[36] by the use of the modified hummer process. In short, 2-g powdered graphite and 18-g potassium permanganate (Aldrich; Sigma) were combined with 40 ml (ratio of 9:1) of concentrated sulfuric acid (98%) (Chem-Supply) and phosphoric acid-85% w/w (Chem-Supply). Then, at 50°C temperature, the as-synthesized solution was mixed for 16 h using a magnetic stirrer and a hot plate. The resulting mixture was consequently cooled down using 20-ml 0.5-M hydrogen peroxide and 400-ml ice cubes. The brownish as-prepared mixture was then centrifuged for 2 h to discard the supernatants and cleaned consecutively with 30% HCl and water. The resulting GO paste was kept in the fridge for further use after removing the supernatants.

2.4 | ZnO nanoparticles incorporated graphene aerogel (3D microstructure) synthesis

The 3D GA microstructure was fabricated by integrating GO into a matrix of sodium alginate (AJAX Chemicals, Australia) by integrating the method of ionic cross-linking and freeze-drying, as stated in our previous work[36] with slight adjustments. In short, first, sodium alginate (4% by weight) was dissolved in distilled water with continuous striation to form a transparent solution. Meanwhile, the GO suspension was ultrasonically dispersed for 20 min to achieve a homogenous distribution. Subsequently, homogeneous GO suspensions were applied to the diluted alginate solution along with recovered ZnO nanoparticles (2% by weight) to achieve various concentration ratios (0, 0.5, 1, 3, and 5 mg/ml), with persistent magnetic stirring, before relatively homogenous dispersion was established. In next step, to fabricate the 3D aerogel microstructure, the coherent GO/Na-ALG solution was transferred into frozen and cold-dried Teflon molding employing freeze dryer. Afterward, 3D aerogel microstructure was submerged in 1-M $CaCl_2$ (Chem-Supply) solution for 1 h to achieve the calcium ion-induced cross-linking phase. After that, once the 3D aerogel microstructure was cross-connected by

calcium ions, the aerogel was washed several times with Milli-Q water (pH = 5.6) to extract the unshackled calcium ions and was cold-dried a further time to establish the cross-linked 3D GA with 12–14 mm decorated dimension with recovered ZnO NPs. (Figure 2A inset).

2.5 | ZnO nanoparticles decorated aerogel graphene structure characterization

The morphological properties of the 3D aerogel graphene formulated with platinum coatings (sputter coated, 3 nm) were analyzed by a scanning electron microscope (SEM) (FEI-QUANTA, Japan), operating at of 20-kV voltage. The transmission electron microscopy (TEM) was carried out using a TECNAI 200, 120-kV microscope device. The crystallographic characterization was carried out using an X-ray diffractometer (XRD, Rigaku).

2.6 | Manufacture of hybrid electrode and asymmetrical supercapacitor

An anode was fabricated by depositing the mi-ZnO–GA (2 cm × 2 cm, precut pressed sample) onto a nickel (Ni) substrate. To create the ohmic contact, precut mi-ZnO–GA and Ni substrate were attached with silver (Ag) paste. A cathode was fabricated by green CVD deposition of ZnO recovered from spent Zn–C battery onto a nickel substrate as a film manner, which is explained in earlier section. Using a separator (Celgard 3501, NC) between the anode and cathode with 0.1-M sodium sulfate (Na_2SO_4) solution as an electrolyte, the ASC was assembled.

2.7 | Electrochemical characterization of individual electrodes

To characterize the electrochemical performance of an individual electrodes (half-cell test), a three-electrode configuration, composing a working electrode, a counter electrode (Pt electrode), and a reference electrode (saturated calomel electrode, SCE), was used.

2.8 | Electrochemical characterization of asymmetric supercapacitors

On an electrochemical workstation, electrochemical impedance spectroscopy measurements, cyclic voltammetry (CV), and charge–discharge actions were carried out for the ASC as-fabricated (CH-Instrument). In particular, the EIS characterizations were carried out using 5-mV AC voltage inside the systems in the frequency 10 mHz to 100 kHz. Two-electrode compositions were directly linked to the anode and cathode of as-fabricated ASC to define the electrochemical features as a complete cell.

3 | RESULTS AND DISCUSSION

3.1 | Characterizations of microrecycled ZnO NPs (mi-ZnO) and microrecycled ZnO thin film (mi-ZnO film) from waste Zn–C batteries

Utilizing field emission SEM (FESEM), TEM, and XRD analysis, as-synthesized recycled ZnO nanoparticles and recycled ZnO thin film were examined. The recycled powder was white–gray, similar in color to the ZnO color produced by the traditional synthesis of zinc acetates or nitrates. The FESEM representation image of synthesized ZnO nanoparticles is shown in Figure 1A. The FESEM surface morphology verified that the restored ZnO particles were in the nano range and comprised nanoparticles in the form of a sphere. The structure of the nanoparticles was almost identical in appearance, and the scale was below 50 nm. Mostly, the particles were distributed homogeneously, although particle accumulation was identified in some regions of the SEM micrographs. The TEM picture (Figure 1A inset) even verified the development of spherical nanoparticles and the size of nanoparticles shown was 10–40 nm. An FESEM microstructure of recycled ZnO NPs deposited in thin film form on the Ni substrate is shown in Figure 1B. In structure, the objects were semispherical and displayed uniform distributions across the substrate as a continuous thin film shape. In all the substrates, the concentration of the nanoparticles was very much the same and the average particle diameter size was ~45 nm. Notably, no accumulation and stacking of particles were found anywhere on the substrate. The optimum conditions, reaction time, and the regulated flow of the gas phase during the experiment[36] could be due to this. A cross-sectional TEM micrograph of the ZnO/Si substrate was used to determine the thickness of both the ZnO ultrathin film and is given in the inset of Figure 1B. The figure shows that ZnO thin film essentially consists of several layers of ZnO film that were periodically stacked with each other and formed one thin sheet. Uniform pores were observed to form between every two layers, rendering the thin film discrete. The thickness of the thin film was roughly ~390 nm, where ~45 nm was the single layer. The amount of thin-film layers could be regulated by adjusting the deposition time. XRD peaks shown in Figure 1C of synthesized ZnO nanoparticles at ~31.67°,

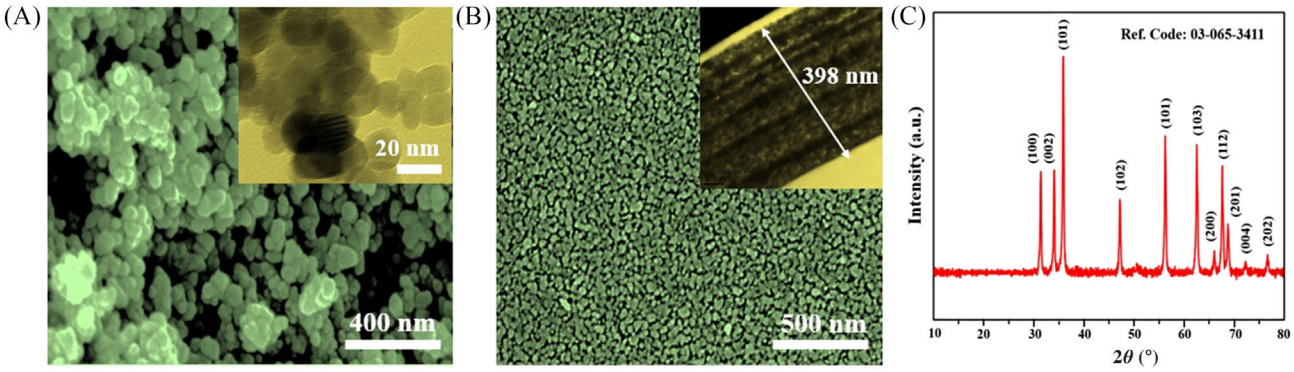

FIGURE 1 (A) Field emission scanning electron microscope (FESEM) image of microrecycled ZnO nanoparticles. (The inset shows the transmission electron microscopy [TEM] of microrecycled ZnO NPs.) (B) FESEM image of a microrecycled ZnO thin film on an Ni substrate. (The inset shows the cross-sectional TEM image of microrecycled ZnO thin film on an Ni substrate.) (C) X-ray diffractometer (XRD) spectra of microrecycled ZnO nanoparticles

34.31°, 36.14°, 47.40°, 56.52°, 62.73°, 66.28°, 67.91°, 69.03°, 72.48°, and 76.96° could be assigned to (1 0 0), (0 0 2), (1 0 1), (1 0 2), (1 0 3), (2 0 0), (1 1 2), (2 0 1), (0 0 4), and (2 0 2) crystallographic planes (Reference code: 03-065-3411). The nanocrystalline existence is indicated by the peaks of as-produced ZnO nanoparticles and corresponds to the pure standard ZnO peaks.[37] As there were no other characteristic impurity peaks, the XRD analysis confirmed the low/no impurities of the ZnO obtained.

3.2 | ZnO nanoparticles embedded graphene oxide aerogel structure characterization

Using FESEM and TEM, morphological analysis of as-synthesized 3D aerogel graphene microstructure and recycled ZnO NPs incorporating 3D aerogel graphene (mi-ZnO–GA) was performed. The uniform 3D microstructure of graphene with associated with internal porosity is shown in Figure 2B. The mean pore size of this 3D pore structure was 60 ± 12 μm, with a variation with the GO concentrations in the composite material of the GO/Na ALG. This is explained by the indications that the association of hydrogen bonding between alginate and GO flakes in the freeze-drying process increases the resistance to the formation of larger ice particles.[38] Figure 2A (inset) shows the optical micrograph of as-fabricated monolithic GA (3D). The FESEM picture of the mi-ZnO–GA cross section (Figure 2B) clearly shows that the ZnO particles (size around 40 nm) distributed consistently on the graphene flakes, indicating sufficient assembly during solvothermal processing between the graphene flakes and the ZnO nanoparticles. Such geometric imprisonment inside the graphene of ZnO NPs prompts the operation and durability of the 3D composite structure.[39] In addition, a TEM has been researching the morphological structure of mi-ZnO–GA. The uniform orientation of ZnO NPs (~40 nm) on the graphene flakes (Figure 2B inset) is further verified by TEM study. The existence of Zn, O, and C elements in the compound is evident from the elemental composition of mZnO–GA (Figure 2C). The as-fabricated mi-ZnO–GA crystalline nature was analyzed by XRD. Figure 2D displays the XRD spectra of 3D crystal structure as fabricated, where all characteristic patterns correlate to ZnO defined (Reference code: 03-065-3411). Notably, in the pattern of the as-synthesized 3D structure, diffraction peaks at 26° corresponding to graphene were observed, suggesting that ZnO nanoparticles were adroitly accumulated on the graphene, resulted in the suppressing of stacking among the layers graphene flakes.[40]

3.3 | Electrochemical performance of mi-ZnO–GA and mi-ZnO thin film electrodes

We have characterized mi-ZnO–GA as an electrode for supercapacitor because of the aerogel configuration, which delivers high surface area. In this study, we performed the electrochemical analysis for the distinct electrodes in a three-electrode system by using 0.1-M sodium sulfate (Na_2SO_4) as an electrolyte, platinum (Pt) as a counter electrode, and SCE as a reference electrode. The concentration of microrecycled ZnO NPs loading was controlled by performing the CV analysis of mi-ZnO–GA fabricated from various mi-ZnO concentrations ranging from 0 to 5 mg/ml (Figure S4). Figure S4 reveals that the GA loaded with 3 mg/ml mi-ZnO displays a larger area in CV curve rather than 5-mg/ml loaded GA due to the enhanced electrical conductivity. In contrast, with the increasing of mi-ZnO within the GA structure causes the reduction of active area

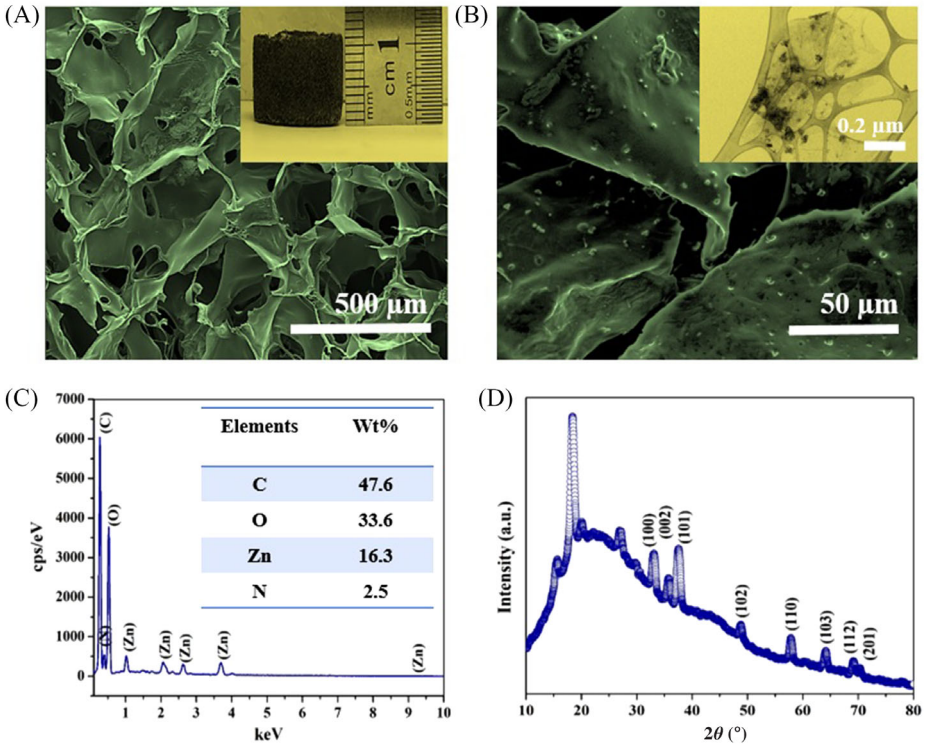

FIGURE 2 (A) Field emission scanning electron microscope (FESEM) image of microstructure three-dimensional graphene aerogel (3D-GA). (The inset shows the optical image of 3D-GA.) (B) FESEM image of a cross section of mi-ZnO–GA. (The inset shows the transmission electron microscopy [TEM] micrograph of mi-ZnO–GA.) (C) EDS spectrum, and (D) X-ray diffractometer (XRD) spectra of mi-ZnO–GA

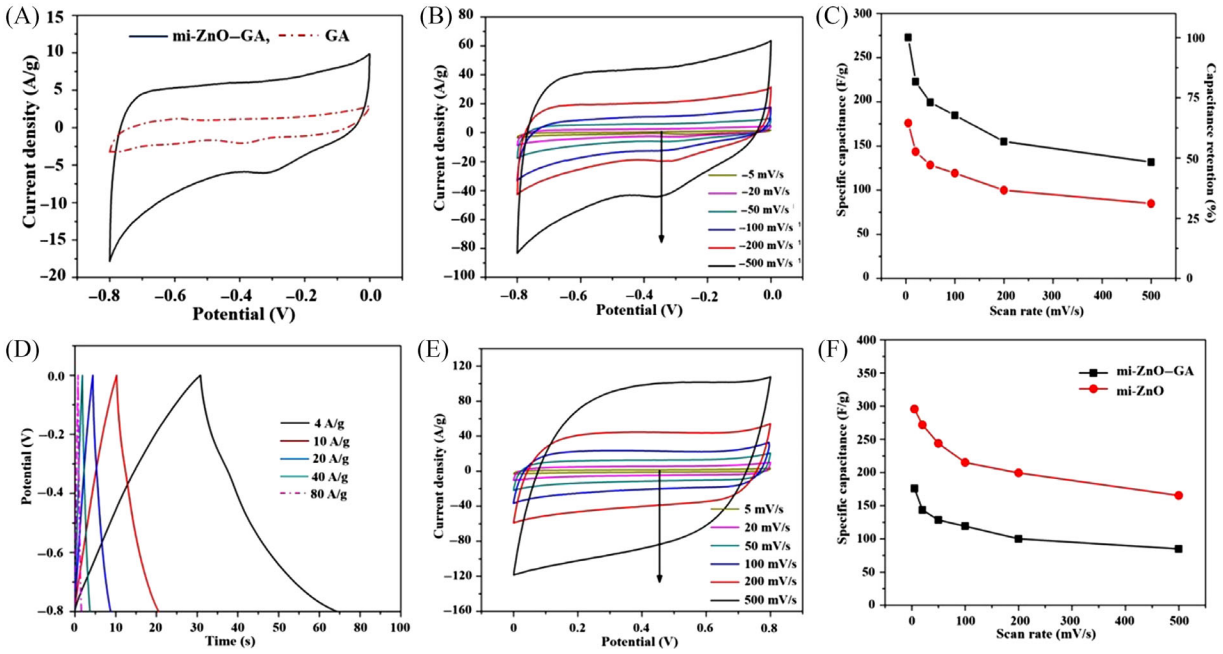

FIGURE 3 (A) Cyclic voltammetry (CV) curves of mi-ZnO–graphene aerogel (GA) and bare GA at a scan rate of 50 mV/s (saturated calomel electrode [SCE] as a reference electrode). (B) CV curves of mi-ZnO–GA at different scan rates ranging from 5 to 500 mV/s (SCE as a reference electrode). (C) Specific capacitance and capacitance retention for the mi-ZnO–GA as a function of scan rates ranging from 0 to 500 mV/s. (D) Galvanostatic charge–discharge (GCD) curves of mi-ZnO–GA at current density from 4 to 80 A/g (SCE as a reference electrode). (E) CV curves of mi-ZnO thin film at scan rates from 5 to 500 mV/s (SCE as a reference electrode). (F) Specific capacitance of mi-ZnO–GA and mi-ZnO thin film as a function of scan rates ranging from 0 to 500 mV/s

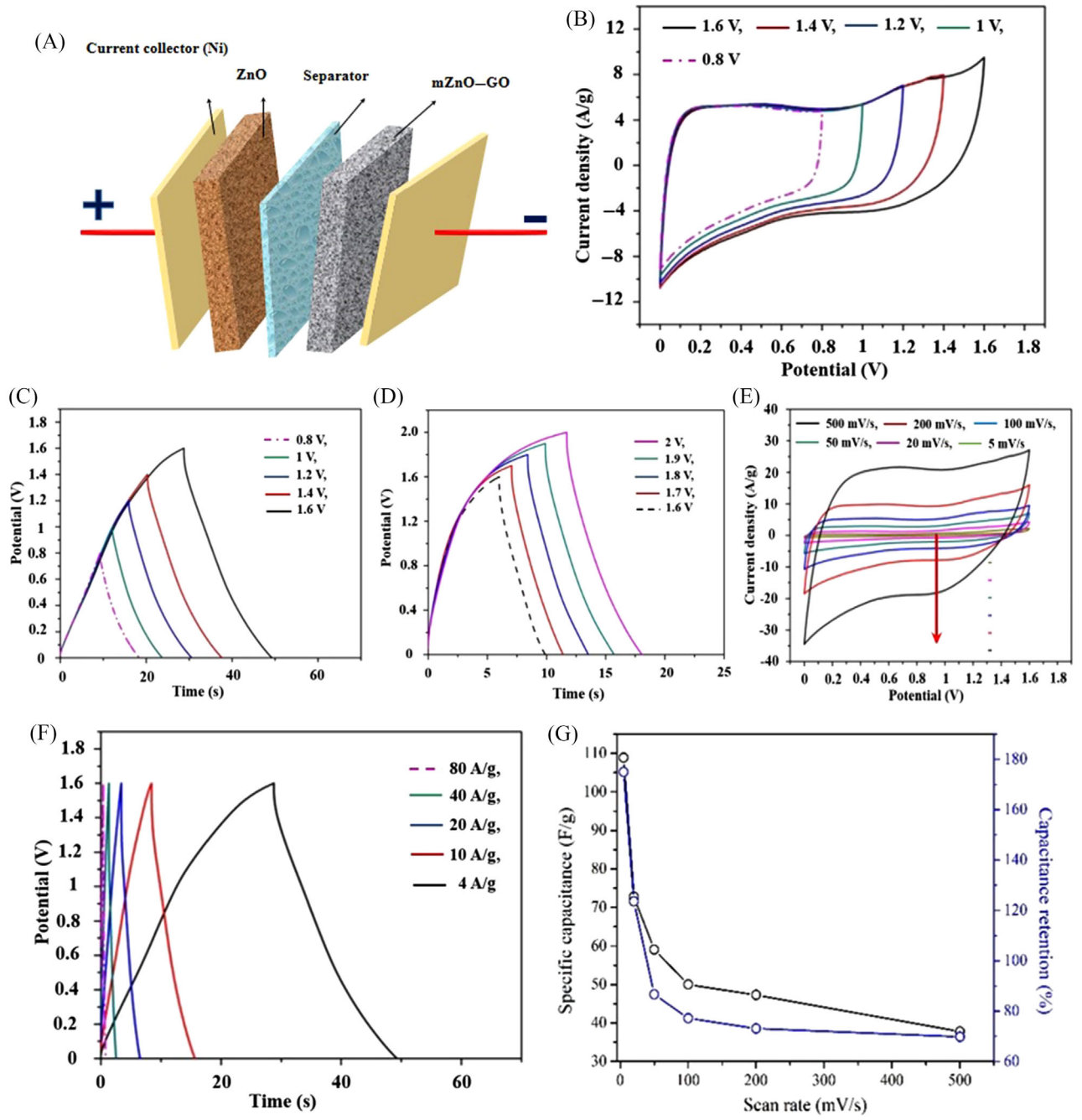

FIGURE 4 (A) Schematic assembled diagram of mi-ZnO film as cathode and mi-ZnO–graphene aerogel (GA) as anode-based asymmetric supercapacitor (ASC). (B) Cyclic voltammetry (CV) curves and (A and D) galvanostatic charge–discharge (GCD) analysis of mi-ZnO//mi-ZnO–GA-based ASC characterized in two electrode systems at different voltage windows. (E) CV curves of mi-ZnO//mi-ZnO–GA-based ASC at different scan rates. (F) GCD curves of mi-ZnO//mi-ZnO–GA-based ASC from 4 to 80 A/g current densities. (G) Specific capacitance and capacitance retention for the mi-ZnO//mi-ZnO–GA-based ASC as a function of scan rates

in CV curve because of the increased weight from mi-ZnO. This was occurred due to the trade-off in between the enhanced electrical conductivity and the added m-ZnO mass. Consequently, we selected a GA with the loading of 3 mg/ml mi-ZnO as the optimum electrode materials for this study. Figure 3A illustrates the CV curve for bare GA and mi-ZnO–GA electrodes at a scan rate of 50 mV/s. Figure 3A reveals that the current density of mi-ZnO–GA has much higher than bare GA electrode, which causes the better electron transportation within mi-ZnO–GA electrodes. Moreover, superior capacitive characteristics of mi-ZnO–GA electrode were observed from the consistent CV curves of mi-ZnO–GA operated at different scan rates ranging from 5 to 500 mV/s with a negative voltage window

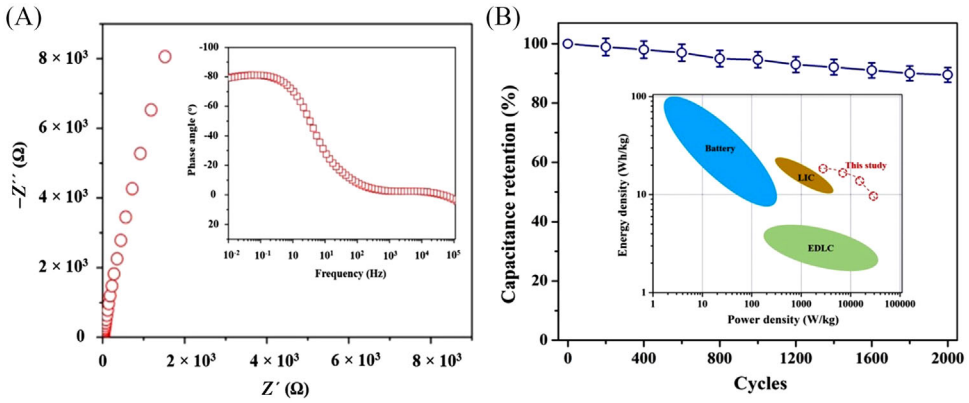

FIGURE 5 (A) Nyquist plot (inset shows the Bode plots) of mi-ZnO//mi-ZnO–graphene aerogel (GA) based asymmetric supercapacitor (ASC). (B) Cycle performance of as-fabricated supercapacitor at a scan rate of 200 mV/s. (The inset illustrates the Ragone plots of as-fabricated supercapacitors comparing with other reported devices.)[5,42]

TABLE 1 Comparison study of different supercapacitors (SCs) in terms of device relaxation time

Materials of SCs	Relaxation time (ms)	References
Carbon aerogel	2000	43
Activated carbon	700	44
MnO_2/carbon composite	500	45
AuPd–MnO_2 core shell	59	46
mi-ZnO//mi-ZnO–GA	233	This study

Abbreviation: GA, graphene aerogel.

(Figure 3B). Figure 3C illustrates the rate performance and specific capacitance of mi-ZnO–GA electrode at different scan rates ranging from 0 to 500 mV/s. From the analysis, it was clearly visible that the specific capacitance of the mi-ZnO–GA electrode (175.8 F/g) was much higher than the bare GA electrode (51.9 F/g). In addition, this as-fabricated electrode displays good rate capability with the retention rate of 48.3% from the base capacitance with the increasing of scan rate ranging from 5° to 500 mV/s. Figure 3D depicts the galvanostatic charge–discharge (GCD) curves for the mi-ZnO–GA electrode and found that the curves are symmetrical in nature at different current densities that suggests the excellent coulombic efficiency as well as superior reversibility. The obtained superior results from the electrochemical analysis of the mi-ZnO–GA electrode imply the potential application of this electros as a negative electrode in the SC device. Meanwhile, mi-ZnO thin film was selected as a positive/cathode material for this study.

Figure 3E illustrates the CV curves of mi-ZnO thin film electrode, which was carried out by using a positive window ranging from 0 to 0.8 V. The CV curve displays constant boxlike profiles as the scan rate increases from 5 to 500 mV/s, suggesting superior capacitive characteristics of mi-ZnO thin film electrode. Figure 3A displays the CV of both mi-ZnO–GA and mi-ZnO thin film electrodes at a scan rate of 50 mV/s. The rectangular profile CV curves for both electrodes employ a voltage window from −0.8 to 0.8 V, suggesting an ASC device composed of these electrodes may have a probable voltage window of 0.6 V. Nevertheless, Figure 3F illustrates the specific capacitance of mi-ZnO–GA (128.5 F/g) and mi-ZnO thin film (243.7 F/g) at 50 mV/s.

3.4 | Electrochemical characterizations of mi-ZnO//mi-ZnO–GA composed asymmetric supercapacitors

In this study, an ASC was fabricated by using microrecycled ZnO thin film (mi-ZnO film) as the positive electrode and microrecycled ZnO NPs incorporated GA (mi-ZnO–GA) as negative electrodes, which was assigned as mi-ZnO//mi-ZnO–GA ASC, as Figure 4A illustrates. Figure 4B illustrates the CV feature curve of as synthesized ASC in 0.1-M sodium sulfate (Na_2SO_4) blend at various voltage measurements at a 100 mV/s constant scanning rate. The synthesized ASC illustrates the quasi-rectangular shape in nature (0.8–1.6 V) alongside a superior capacitive nature, which proves the practicability of mi-ZnO film and mi-ZnO–GA as positive and negative electrodes, respectively. Further, GCD characteristics behavior also analyzed of this as-fabricated ASC along with CV to ensure the possibility as a freestanding tool. The as synthesized ASC's GCD curves at a current density of 4 A/g with a voltage window between 0.8 and 1.6 V are represented in Figure 4C. It was observed from the figure that the curve represents a balanced triangular pattern (up until 1.6 V), which was an indication of the as synthesized ASC device's stable electrochemical voltage.

TABLE 2 Comparison study in terms of power density and the average energy density of various asymmetric supercapacitors (ASCs)

Materials of ASCs	Average energy density (W h/kg)	Power density (kW/kg)	Electrolyte	Specific capacitance (F/g)	References
MnO_2 NW-graphene//graphene	7.2	5	Na_2SO_4	24.5 @ 10 mV/s	47
Nickel hydroxide-graphite//activated graphene ($Ni(OH_2$-graphite//AGO)	6.9	44	KOH	106 @ 5 mV/s	48
Reduced graphene oxide-ruthenium oxide//reduced graphene oxide-polyaniline (RGO-RuO_2//(RGO-PANI)	6.7	50	H_2SO_4	357 @ 50 mV/s	49
Graphene-MnO_2//activated carbon nanofiber (graphene-MnO_2//ACN	10	12	Na_2SO_4	211 @ 10 mV/s	50
MnO_2//graphene hydrogel (MnO_2//GH	14.9	10	Na_2SO_4	41.7 @ 5 mV/s	21
Mo-doped ZnO nanoflakes	39.06	7.42	HCl and NF	123 @1 A/g	51
Honeycomb-like ZnO/SnO_2 nanocomposite on Ni foam	47.28	10.4	KOH	133 @ 1 mV/s	52
Microrecycled ZnO thin film// microrecycled ZnO incorporated GA (mi-ZnO//mi-ZnO–GA)	13.7	13.2	Na_2SO_4	108.95 mV/s	Present study

Abbreviation: GA, graphene aerogel.

Nevertheless, in this study, an as-fabricated ASC device is also analyzed with greater voltage measurement up until 2 V and has been noticed that the GCD curves become asymmetrical, which markedly lessens the reversibility performance of the as synthesized ASCs material. That is why, in this study, further characterizations were performed by considering voltage measurement up until 1.6-V limit. The illustrations in Figure 4E represent the CV features curve of mi-ZnO//mi-ZnO–GA ASC characterized at numerous scanning rates, that is, 5, 20, 50, 100, 200, and 500 mV/s, where the voltage limit is a constant parameter (1.6 V). The CV curves did not represent any redox peaks, which point out the ideal capacitive characteristics of as-fabricated ASC. Besides, described the CV curves for as synthesized ASC materials continued as a rectangular shape manner with amplified scanning rates (500 from 5 mV/s) by presentation without any distortion, which open up the window for as-fabricated ASC as a fast charging/discharging power device for real application. GCD performance curves of mi-ZnO//mi-ZnO–GA based ASC likewise presented at various current densities in the range between 4 and 80 A/g as represented in Figure 4F. Its efficient capacitive behavior is verified by the symmetrical behavior of the GCD profiles. Relevantly, at a scanning rate of 5 mV/s, 108.9 F/g specific capacitance (SC_{max}) was measured for as-synthesized ASC (Figure 4G). In addition, it is worth noting that the as-synthesized ASC's specific capacitance remains at 37.8 F/g and that is with the increased scanning rate at 500 mV/s together with capacitance retaining of up until 34.7% (Figure 4G).

The electrochemical efficiency of the mi-ZnO/mi-ZnO–GA ASC was again defined within a wide frequency range by the electrochemical impedance spectroscope (from 10 mHz to 100 kHz). Figure 5A illustrates the Nyquist plot of as-fabricated ASC, and it was found that the curve was straight in nature, which was obvious for the as-fabricated device's ideal capacitive behavior. It is worth noting that the measured resistance of the ASC on the real axis was similar to the intercept of the Nyquist plot, which reflects the electrolyte's strong conductivity and lower resistivity. Moreover, for the as-fabricated ASC, Bode characteristics curve was plotted and it was found that phase angle was nearly ~90° within the frequency of 1 Hz. This results reveal that the ideal capacitive behavior of as-fabricated ASC with a relaxation time 233 ms (4.29 Hz, ~45°) was measured, where, at certain point, resistance and capacitive impedance are equal.[41] Compared to other recorded time constants for SCs from previous literature, this remarkable short time

constant for the mi-ZnO/mi-ZnO–GA ASC is competitive (Table 1).

For an energy storage device, cycling stability is very important parameters for characterizing their performances. Figure 5B illustrates the cycling behavior of mi-ZnO//mi-ZnO–GA ASC as an energy storage device at 200-mV/s scan rate. From the analysis, it was evident that, after 5000 cycles, the capacitance of as-fabricated ASC still remains 76.8% comparing with its primary value and proved the significant cycling stability. With the exception of this cycling durability, the characteristics of power density and energy density are also important for assessing energy storage systems. The measured energy density and power density were 13.7 W h/kg and 13.2 kW/kg for mi-ZnO/mi-ZnO–GA ASC, which was superior/competitive to other published ASC performance (Table 2). Moreover, the inset of Figure 5B displays the Ragone plots, which represents the comparison of our as-fabricated ASC to batteries as well as lithium-ion capacitors (LIC). The results indicate the comparable energy density region along with superior power density region to batteries and LICs. In addition, these as-synthesized systems had a region of power density comparable to an electrochemical double-layer capacitor and superior energy density region. However, these groundbreaking outcomes for mi-ZnO–GA may lead to other real application (e.g., sensing and catalysis)

4 | CONCLUSIONS

Throughout this research, the sustainable and environment-friendly synthetic fabrication approach to the synthesis of aerogel graphene integrated with ZnO nano materials was established, which could potentially be utilized for anode materials in fabricating highly efficient ASCs. As-produced macroporous composites (3D), nanoparticles not just exhibit uniform arrangement, but they also show an intimate interaction between both the recycled ZnO nanoparticles and graphene flakes to construct heterostructure areas at the interfaces. Relevantly, along with a wide surface region, 3D graphene demonstrates integrated macroporous networks, providing flexible, versatile, fast ion transport pathways. Finally, as an outcome, high-performance ASC was fabricated by configuring recycled ZnO thin film as a cathode and recycled ZnO nanoparticles integrated aerogel graphene as an anode material. The as-synthesized ASC shows improved energy and power densities of 13.2 kW/kg and 13.7 W h/kg, respectively. These results are significantly enhanced than other devices reported for ASC. Nevertheless, the arrangement of the mi-ZnO–GA materials used for the anode of ASCs open up the window for energy storing devices with excellent energy and power densities.

ACKNOWLEDGMENTS

This research was supported by the Australian Research Council's Industrial Transformation Research Hub funding scheme (project IH190100009).

Open access publishing facilitated by University of New South Wales, as part of the Wiley - University of New South Wales agreement via the Council of Australian University Librarians.

CONFLICT OF INTEREST

The authors declare no competing financial interest.

ORCID

Rumana Hossain https://orcid.org/0000-0002-5585-931X

REFERENCES

1. Miller JR, Simon P. Electrochemical capacitors for energy management. Sci Mag. 2008;321(5889):651–2.
2. Hou Y, Cheng Y, Hobson T, Liu J. Design and synthesis of hierarchical MnO_2 nanospheres/carbon nanotubes/conducting polymer ternary composite for high performance electrochemical electrodes. Nano Lett. 2010;10(7):2727–33.
3. Simon P, Gogotsi Y. Materials for electrochemical capacitors. nanoscience and technology: a collection of reviews from nature journals. Singapore: World Scientific; 2010. p. 320–9.
4. Yu Z, Duong B, Abbitt D, Thomas J. Highly ordered MnO_2 nanopillars for enhanced supercapacitor performance. Adv Mater. 2013;25(24):3302–6.
5. Wang G, Zhang L, Zhang J. A review of electrode materials for electrochemical supercapacitors. Chem Soc Rev. 2012;41(2):797–828.
6. Stoller MD, Ruoff RS. Best practice methods for determining an electrode material's performance for ultracapacitors. Energy Environ Sci. 2010;3(9):1294–301.
7. Demarconnay L, Raymundo-Piñero E, Béguin F. Adjustment of electrodes potential window in an asymmetric carbon/MnO_2 supercapacitor. J Power Sources. 2011;196(1):580–6.
8. Lewandowski A, Olejniczak A, Galinski M, Stepniak I. Performance of carbon–carbon supercapacitors based on organic, aqueous and ionic liquid electrolytes. J Power Sources. 2010;195(17):5814–9.
9. Duong B, Yu Z, Gangopadhyay P, Seraphin S, Peyghambarian N, Thomas J. High throughput printing of nanostructured carbon electrodes for supercapacitors. Adv Mater Interfaces. 2014;1(1):1300014.
10. Chen P-C, Shen G, Shi Y, Chen H, Zhou C. Preparation and characterization of flexible asymmetric supercapacitors based on transition-metal-oxide nanowire/single-walled carbon nanotube hybrid thin-film electrodes. ACS Nano. 2010;4(8):4403–11.
11. Xiao X, Li T, Peng Z, Jin H, Zhong Q, Hu Q, et al. Freestanding functionalized carbon nanotube-based electrode for solid-state asymmetric supercapacitors. Nano Energy. 2014;6:1–9.

12. Yang P, Ding Y, Lin Z, Chen Z, Li Y, Qiang P, et al. Low-cost high-performance solid-state asymmetric supercapacitors based on MnO_2 nanowires and Fe_2O_3 nanotubes. Nano Lett. 2014;14(2):731–6.
13. Wang D-W, Li F, Cheng H-M. Hierarchical porous nickel oxide and carbon as electrode materials for asymmetric supercapacitor. J Power Sources. 2008;185(2):1563–8.
14. Yan J, Fan Z, Sun W, Ning G, Wei T, Zhang Q, et al. Advanced asymmetric supercapacitors based on Ni(OH)2/graphene and porous graphene electrodes with high energy density. Adv Funct Mater. 2012;22(12):2632–41.
15. Zhou C, Zhang Y, Li Y, Liu J. Construction of high-capacitance 3D CoO@ polypyrrole nanowire array electrode for aqueous asymmetric supercapacitor. Nano Lett. 2013;13(5):2078–85.
16. Wang X, Yan C, Sumboja A, Lee PS. High performance porous nickel cobalt oxide nanowires for asymmetric supercapacitor. Nano Energy. 2014;3:119–26.
17. Chen LF, Huang ZH, Liang HW, Guan QF, Yu SH. Bacterial-cellulose-derived carbon nanofiber@MnO_2 and nitrogen-doped carbon nanofiber electrode materials: an asymmetric supercapacitor with high energy and power density. Adv Mater. 2013;25(34):4746–52.
18. Jiang H, Li C, Sun T, Ma J. A green and high energy density asymmetric supercapacitor based on ultrathin MnO_2 nanostructures and functional mesoporous carbon nanotube electrodes. Nanoscale. 2012;4(3):807–12.
19. Sumboja A, Foo CY, Wang X, Lee PS. Large areal mass, flexible and free-standing reduced graphene oxide/manganese dioxide paper for asymmetric supercapacitor device. Adv Mater. 2013;25(20):2809–15.
20. Chen P, Yang J-J, Li S-S, Wang Z, Xiao T-Y, Qian Y-H, et al. Hydrothermal synthesis of macroscopic nitrogen-doped graphene hydrogels for ultrafast supercapacitor. Nano Energy. 2013;2(2):249–56.
21. Gao H, Xiao F, Ching CB, Duan H. High-performance asymmetric supercapacitor based on graphene hydrogel and nanostructured MnO_2. ACS Appl Mater Interfaces. 2012;4(5):2801–10.
22. Cao X, Yin Z, Zhang H. Three-dimensional graphene materials: preparation, structures and application in supercapacitors. Energy Environ Sci. 2014;7(6):1850–65.
23. Cong H, Ren X, Wang P, Yu S. Macroscopic multifunctional graphene-based hydrogels and aerogels by a metal ion induced self-assembly process. ACS Nano. 2012;6:2693–703.
24. Yun S, Kang S-O, Park S, Park HS. CO_2-activated, hierarchical trimodal porous graphene frameworks for ultrahigh and ultrafast capacitive behavior. Nanoscale. 2014;6(10):5296–302.
25. Zhu Y, Murali S, Cai W, Li X, Suk JW, Potts JR, et al. Graphene and graphene oxide: synthesis, properties, and applications. Adv Mater. 2010;22(35):3906–24.
26. Okamoto Y. Density-functional calculations of icosahedral M13 (M = Pt and Au) clusters on graphene sheets and flakes. Chem Phys Lett. 2006;420(4–6):382–6.
27. Macedo LJ, Iost RM, Hassan A, Balasubramanian K, Crespilho FN. Bioelectronics and interfaces using monolayer graphene. ChemElectroChem. 2019;6(1):31–59.
28. Kumar R, Varandani D, Mehta B, Singh V, Wen Z, Feng X, et al. Fast response and recovery of hydrogen sensing in Pd–Pt nanoparticle–graphene composite layers. Nanotechnology. 2011;22(27):275719.
29. Shah MA, Batool R. An overview of electronic waste management, practices and impending challenges. Int J Comput Appl. 2015;975:8887.
30. Farzana R, Rajarao R, Behera PR, Hassan K, Sahajwalla V. Zinc oxide nanoparticles from waste Zn-C battery via thermal route: characterization and properties. Nanomaterials. 2018;8(9):717.
31. Ebin B, Petranikova M, Steenari B-M, Ekberg C. Production of zinc and manganese oxide particles by pyrolysis of alkaline and Zn–C battery waste. Waste Manage (Oxford). 2016;51:157–67.
32. Charef SA, Affoune A, Caballero A, Cruz-Yusta M, Morales J. Simultaneous recovery of Zn and Mn from used batteries in acidic and alkaline mediums: a comparative study. Waste Manage (Oxford). 2017;68:518–26.
33. Deep A, Sharma AL, Mohanta GC, Kumar P, Kim K-H. A facile chemical route for recovery of high quality zinc oxide nanoparticles from spent alkaline batteries. Waste Manage (Oxford). 2016;51:190–5.
34. Farzana R, Rajarao R, Hassan K, Behera PR, Sahajwalla V. Thermal nanosizing: novel route to synthesize manganese oxide and zinc oxide nanoparticles simultaneously from spent Zn–C battery. J Cleaner Prod. 2018;196:478–88.
35. Hassan K, Farzana R, Sahajwalla V. In-situ fabrication of ZnO thin film electrode using spent Zn–C battery and its electrochemical performance for supercapacitance. SN Appl Sci. 2019;1(4):302.
36. Hassan K, Hossain R, Sahajwalla V. Novel microrecycled ZnO nanoparticles decorated macroporous 3D graphene hybrid aerogel for efficient detection of NO2 at room temperature. Sens Actuators B. 2021;330:129278.
37. Zhang J, Zhao B, Pan Z, Gu M, Punnoose A. Synthesis of ZnO nanoparticles with controlled shapes, sizes, aggregations, and surface complex compounds for tuning or switching the photoluminescence. Cryst Growth Des. 2015;15(7):3144–9.
38. Murphy CM, Haugh MG, O'brien FJ. The effect of mean pore size on cell attachment, proliferation and migration in collagen–glycosaminoglycan scaffolds for bone tissue engineering. Biomaterials. 2010;31(3):461–6.
39. Liang J, Wei W, Zhong D, Yang Q, Li L, Guo L. One-step in situ synthesis of SnO2/graphene nanocomposites and its application as an anode material for Li-ion batteries. ACS Appl Mater Interfaces. 2012;4(1):454–9.
40. Wu Z-S, Yang S, Sun Y, Parvez K, Feng X, Müllen K. 3D nitrogen-doped graphene aerogel-supported Fe3O4 nanoparticles as efficient electrocatalysts for the oxygen reduction reaction. J Am Chem Soc. 2012;134(22):9082–5.
41. Taberna P, Simon P, Fauvarque J-F. Electrochemical characteristics and impedance spectroscopy studies of carbon-carbon supercapacitors. J Electrochem Soc. 2003;150(3):A292.
42. Yu Z, Li C, Abbitt D, Thomas J. Flexible, sandwich-like Ag-nanowire/PEDOT: PSS-nanopillar/MnO 2 high performance supercapacitors. J Mater Chem A. 2014;2(28):10923–9.
43. Rasines G, Lavela P, Macías C, Haro M, Ania C, Tirado J. Electrochemical response of carbon aerogel electrodes in saline water. J Electroanal Chem. 2012;671:92–8.
44. Pech D, Brunet M, Durou H, Huang P, Mochalin V, Gogotsi Y, et al. Ultrahigh-power micrometre-sized supercapacitors based on onion-like carbon. Nat Nanotechnol. 2010;5(9):651–4.

45. Yuan L, Lu X-H, Xiao X, Zhai T, Dai J, Zhang F, et al. Flexible solid-state supercapacitors based on carbon nanoparticles/MnO_2 nanorods hybrid structure. ACS Nano. 2012;6(1):656–61.
46. Yu Z, Thomas J. Energy storing electrical cables: integrating energy storage and electrical conduction. Adv Mater. 2014;26(25):4279–85.
47. Wu Z, Ren W, Wang D, Li F, Liu B, Cheng H. High-energy MnO_2 nanowire/graphene graphene asymmetric electrochemical capacitors. ACS Nano. 2010;4(10):5835–42.
48. Ji J, Zhang LL, Ji H, Li Y, Zhao X, Bai X, et al. Nanoporous Ni (OH) 2 thin film on 3D ultrathin-graphite foam for asymmetric supercapacitor. ACS Nano. 2013;7(7):6237–43.
49. Zhang J, Jiang J, Li H, Zhao X. A high-performance asymmetric supercapacitor fabricated with graphene-based electrodes. Energy Environ Sci. 2011;4(10):4009–15.
50. Fan Z, Yan J, Wei T, Zhi L, Ning G, Li T, et al. Asymmetric supercapacitors based on graphene/MnO_2 and activated carbon nanofiber electrodes with high power and energy density. Adv Funct Mater. 2011;21(12):2366–75.
51. Ali A, Ammar M, Ali M, Yahya Z, Javaid MY, Hassan SU, et al. Mo-doped ZnO nanoflakes on Ni-foam for asymmetric supercapacitor applications. RSC Adv. 2009;9:27432–8.
52. Ali M, Ammar M, Yahya Z, Waqas M, Jamal MA, Slhabi EHM. A honeycomb-like ZnO/SnO_2 nanocomposite on nickel foam for high-performance asymmetric supercapacitors. New. J. Chem. 2019;43: 10583–9.

SUPPORTING INFORMATION

Additional supporting information can be found online in the Supporting Information section at the end of this article.

How to cite this article: Hassan K, Hossain R, Sahajwalla V. Recycled ZnO-fused macroporous 3D graphene oxide aerogel composites for high-performance asymmetric supercapacitors. J Am Ceram Soc. 2022;105:7467–7478. https://doi.org/10.1111/jace.18697